
Supervised Graph Contrastive Learning for Gene Regulatory Network

Sho Oshima*

Graduate School of Medicine
Kyoto University
Kyoto, 606-8501
oshima.sho.44a@st.kyoto-u.ac.jp

Yuji Okamoto*

Graduate School of Medicine
Kyoto University
Kyoto, 606-8501
okamoto.yuji.2c@kyoto-u.ac.jp

Taisei Tosaki

Graduate School of Medicine
Kyoto University
Kyoto, 606-8501
tosaki.taisei.77a@st.kyoto-u.ac.jp

Ryosuke Kojima

Graduate School of Medicine
Kyoto University
Kyoto, 606-8501
kojima.ryosuke.8e@kyoto-u.ac.jp

Yasushi Okuno

Graduate School of Medicine
Kyoto University
Kyoto, 606-8501
okuno.yasushi.4c@kyoto-u.ac.jp

Abstract

Graph representation learning is effective for obtaining a meaningful latent space utilizing the structure of graph data and is widely applied, including biological networks. In particular, Graph Contrastive Learning (GCL) has emerged as a powerful self-supervised method that relies on applying perturbations to graphs for data augmentation. However, when applying existing GCL methods to biological networks such as Gene Regulatory Networks (GRNs), they overlooked meaningful biologically relevant perturbations, e.g., gene knockdowns. In this study, we introduce SupGCL (Supervised Graph Contrastive Learning), a novel GCL method for GRNs that directly incorporates biological perturbations derived from gene knockdown experiments as the supervision. SupGCL mathematically extends existing GCL methods that utilize non-biological perturbations to probabilistic models that introduce actual biological gene perturbation utilizing gene knockdown data. Using the GRN representation obtained by our proposed method, our aim is to improve the performance of biological downstream tasks such as patient hazard prediction and disease subtype classification (graph-level task), and gene function classification (node-level task). We applied SupGCL on real GRN datasets derived from patients with multiple types of cancer, and in all experiments SupGCL achieves better performance than state-of-the-art baselines.

1 Introduction

Graph representation learning has recently attracted attention in various fields to learn a meaningful latent space to represent the connectivity and attributes in given graphs [1]. Applications of graph

*Equal Contribution

representation learning are advancing in numerous areas where network data exists, such as analysis in social networks, knowledge graphs [2, 3], and biological network analysis in bioinformatics [4, 5].

Among these applications, the use of graph representation learning for Gene Regulatory Networks (GRNs), where each node and edge represents important intracellular functions and/or processes, is particularly significant in the fields of biology and drug discovery, as it is expected to contribute to identifying therapeutic targets and understanding disease mechanisms. GRN representation learning has been applied to tasks such as inferring transcription factors [6] and predicting drug responses in cancer cell lines [7].

With advancements in gene expression measurement and analysis technologies, identification methods for GRNs from expression data are also evolving. Traditional GRN identification constructs networks using statistical techniques applied to patient populations. Recently, it has become possible to construct GRNs specific to individual patients, highlighting distinct gene regulatory patterns compared to the population as a whole [8]. Hereafter in this paper, we refer to such individualized networks simply as GRNs. Similarly, in cell-based experiments such as gene knockdowns, it is now possible to estimate distinct GRNs for each experiment depending on the expression profile.

Graph representation learning applied to GRNs is believed to be effective for a wide range of biological applications. Among such methods, Graph Contrastive Learning (GCL) has gained traction. GCL enhances graph data via artificial perturbations applied to nodes or edges, and learns useful graph embeddings by maximizing the similarity between differently augmented views of the same graph [9]. For example, we can perform contrastive learning by artificial perturbations such as randomly removing nodes to augment the GRN and consequently learn a representation for the GRN.

However, a major challenge arises in that the artificial perturbations employed in conventional GCL methods significantly deviate from genuine biological perturbations, making it difficult to learn effective representations when applied to GRNs. A related issue occurs in heterogeneous node networks, where random perturbations to nodes or edges during augmentation can disrupt topology and attribute integrity, ultimately hindering representation learning [10, 11]. This problem is especially relevant to GRNs, where node heterogeneity exists—for example, in the presence of master regulators [12].

To address these issues, we propose a novel supervised GCL method (SupGCL) that leverages gene knockdown perturbations within GRNs. Our method uses experimental data from actual gene knockdowns as supervision, enabling biologically faithful representation learning. In gene knockdown experiments, the expression of specific genes is suppressed, representing biological perturbations that allow for the inference of GRNs. By using these perturbations as supervision signals for GCL, we can perform data augmentation that retains biological characteristics. Moreover, since our method naturally extends traditional GCL models in the direction of supervised augmentation within a probabilistic framework, conventional GCL approaches emerge as special cases of our proposed model.

To evaluate the effectiveness of the proposed SupGCL method, we apply it to GRN datasets from cancer patients across three cancer types and conduct multiple downstream tasks. For gene-level downstream tasks, we perform classification into Biological Process, Cellular Component, and cancer-related gene categories. For patient-level tasks, we conduct hazard prediction and disease subtype classification. The performance of our method is compared against existing graph representation learning techniques, including conventional GCL methods.

The main contributions of this study are as follows:

- **Proposal of a novel GRN representation learning method utilizing gene knockdown experiments:** We develop a new GCL method tailored for GRNs that incorporates gene knockdown data as supervision to enhance biological plausibility.
- **Theoretical extension of GCL:** We formulate supervised GCL, incorporating augmentation selection into a unified probabilistic modeling framework, and theoretically demonstrate that existing GCL methods are special cases of our proposed approach.
- **Empirical validation of the proposed method:** We apply the method to 13 downstream tasks on GRNs derived from real cancer patients and consistently outperform conventional approaches across all tasks.

Our implementation and all experimental codes are available on <http://github.com/xxxxxx>.

2 Related Work

Graph Contrastive Learning (GCL) has inspired the development of numerous methods, largely based on the design of data augmentations and the construction of positive/negative sample pairs [10]. GCL methods can be broadly categorized into three types according to how they generate these training pairs: (1) graph-level pairs, (2) node-level pairs, and (3) cross-model pairs.

A representative method using graph-level pairs is GraphCL [13], which applies random data augmentations to graphs and treats the resulting two graph views as a positive pair. This approach enhances the model’s ability to capture graph-level representations. However, it has been pointed out that node-level information can become obscured in the process [14]. This limitation is especially problematic in applications like Gene Regulatory Networks (GRNs), where the semantics of individual nodes are crucial.

In contrast, methods such as GRACE, which generate node-level pairs, apply augmentations to graphs and treat embeddings of different nodes as negative pairs during training [15]. This enables more precise representation learning that captures local structure and attribute information at the node level. Although GRACE has been applied to real GRNs [6], the augmentation strategies used do not incorporate the specific biological characteristics of GRNs.

Beyond direct graph manipulations, methods like BGRL [16] generate positive pairs across models—between two instances of the same graph embedding model operating at different learning speeds—rather than relying on heuristic graph augmentations. Such cross-model pairing strategies have attracted attention for their ability to learn graph representations in a more natural manner. Notably, the recently proposed SGRL [17] achieves stable and high-performance self-supervised learning by using a pair of models: one that distributes node embeddings uniformly on a hypersphere, and another that incorporates graph topology information. However, these methods are constrained by their inability to design task-specific perturbations, and their applicability to biological networks such as GRNs remains unexplored and unverified.

3 Preliminaries

3.1 Background of Graph Contrastive Learning

Although there are various definitions of contrastive learning, it can be expressed using a probabilistic model based on KL divergence over pairs of augmentations or node instances [18]. Let \mathcal{X} denote a set of entities and let $(x, y) \in \mathcal{X} \times \mathcal{X}$ be a pair from that set. The contrastive loss is formulated as follows:

$$\text{LOSS}_{\text{CON}} \triangleq \frac{1}{|\mathcal{X}|} \sum_{x \in \mathcal{X}} D_{\text{KL}}(p_{\theta}(y|x) | q_{\phi}(y|x)). \quad (1)$$

Here, $q_{\phi}(y|x)$ is the probability distribution of the target model with parameter ϕ , and $p_{\theta}(y|x)$ is a reference distribution. To avoid trivial solutions when training both p_{θ} and q_{ϕ} simultaneously, the reference distribution p_{θ} is almost fixed. The reference model $p_{\theta}(y|x)$ is often designed as a probability that assigns a non-zero constant to positive pairs (x, y) and zero to negative pairs (x, y) .

Graph Contrastive Learning (GCL) handles the target model $q_{\phi}(j|i)$ corresponding to a pair of nodes (i, j) . Consider graph operations for augmentation, order them, and represent the index of these operations by a . Let $z_i^a \in \mathbb{R}^d$ be the graph embedding of the i -th node obtained from the Graph Neural Network under the a -th augmentation operation. For two augmentation operations (a, b) , the pair of probability models $(p, q_{\phi}^{a,b})$ used in GCL is defined by

$$p(j|i) \triangleq \delta_{ij}, \quad q_{\phi}^{a,b}(j|i) \triangleq \frac{\exp(\text{sim}(z_i^a, z_j^b)/\tau_n)}{\sum_{k \in \mathcal{V}} \exp(\text{sim}(z_i^a, z_k^b)/\tau_n)}. \quad (2)$$

Here, \mathcal{V} is the set of nodes in the given graph, δ_{ij} is the Dirac delta, $\tau_n > 0$ is a temperature parameter and $\text{sim}(\cdot, \cdot)$ denotes cosine similarity. This setting is often extended so that the definitions of $(p, q_{\phi}^{a,b})$

vary according to how positive and negative pairs are sampled. Note that the target model q_ϕ depends on the sampling method of augmentation operators, so the probability model also depends on (a, b) .

GCL trains the model using the following loss function on the pair of probability models $(p, q_\phi^{a,b})$ induced by augmentation operations (a, b) , according to the formulation of contrastive learning loss (1).

$$\text{Loss}_{\text{node}}^{a,b} \triangleq \frac{1}{|\mathcal{V}|} \sum_{i \in \mathcal{V}} D_{\text{KL}}(p(j|i) | q_\phi^{a,b}(j|i)). \quad (3)$$

This encourages the embeddings at the node level z_i^a and z_i^b of the same node under different augmentation operations to be close to each other. Typically, augmentation operations a, b are chosen by uniform sampling from a set of candidates \mathcal{A} . Hence, in practice, the expected value is minimized under the uniform distribution $U_{\mathcal{A}}$ over \mathcal{A} :

$$\text{Loss}_{\text{node}} \triangleq \mathbb{E}_{a,b \sim U_{\mathcal{A}}} [\text{Loss}_{\text{node}}^{a,b}]. \quad (4)$$

While GCL achieves node-level representation learning via the procedure described above, in many cases the augmentation operations themselves rely on artificial perturbations such as randomly adding and/or deleting nodes and/or edges. In this study, we introduce gene knockdown—a biological perturbation—as supervision for these augmentation operations.

3.2 Notation and Problem Definition

In this study, we describe a GRN as a directed graph $\mathcal{G} \triangleq (\mathcal{V}, \mathcal{E}, X^{\mathcal{V}}, X^{\mathcal{E}})$ that contains information on nodes and edges. Here, \mathcal{V} , and \mathcal{E} are the sets of nodes and edges, respectively, and each node represents a gene. $X_i^{\mathcal{V}}$ is the feature of the i -th gene, and $X_i^{\mathcal{E}} \in \mathbb{R}^{|\mathcal{E}|}$ is the feature of the i -th edge in the network. The augmentation operation corresponding to the knockdown of the i -th gene is modeled by setting the feature of the i -th gene to zero and also setting the features of all edges connected to the i -th gene to zero.

We associate the a -th augmentation operation with the knockdown of the a -th gene. In what follows, we denote by \mathcal{G}_a the graph obtained by applying the a -th augmentation operation to \mathcal{G} . Moreover, in this study, let \mathcal{H}_a be the teacher GRN for the knockdown of the a -th gene, and let \mathcal{K} be the set of all augmentation operations for which such teacher GRNs exist. In other words, \mathcal{H}_a is a GRN that serves as a teacher for artificial augmentation for the a -th gene.

Our goal is to use the original GRN \mathcal{G} and its teacher GRNs $\{\mathcal{H}_a\}_{a \in \mathcal{K}}$ to train a Graph Neural Network (GNN) f_ϕ . Defining embedded representations through the GNN f_ϕ as

$$Z^a \triangleq f_\phi(\mathcal{G}_a) \in \mathbb{R}^{|\mathcal{V}| \times d}, \quad Y^a \triangleq f_\phi(\mathcal{H}_a) \in \mathbb{R}^{|\mathcal{V}| \times d}, \quad (5)$$

where z_i^a and y_i^a denote the embedding vectors of the i -th node in Z^a and Y^a , respectively, and d is the embedding dimension. Note that the same GNN f_ϕ is used to produce both Z^a and Y^a .

In this work, we train the neural network f_ϕ using the set of pairs $\{(Z^a, Y^a)\}_{a \in \mathcal{K}}$, where (Z^a, Y^a) corresponds to the graph embedding obtained by the GRN augmentation operation and the embedding of the teacher GRN for the corresponding gene knockdown.

4 Method

For the set of embedded representations $\{(Z^a, Y^a)\}_{a \in \mathcal{K}}$, we consider the pair of augmentation operations (a, b) and the pair of nodes (i, j) according to the contrastive learning scheme. First, for the pair of augmentation operations (a, b) , we clarify the supervised learning problem for augmentation operations using KL divergence and then propose SupGCL using a distribution over pairs of combinations of nodes and extension operations. A sketch of the proposed method is shown in Figure 1.

The probability distribution of augmentation operations is naturally introduced by using similarities in the entire graph embedding space $\mathbb{R}^{|\mathcal{V}| \times d}$ (rather than per node). By introducing the Frobenius inner

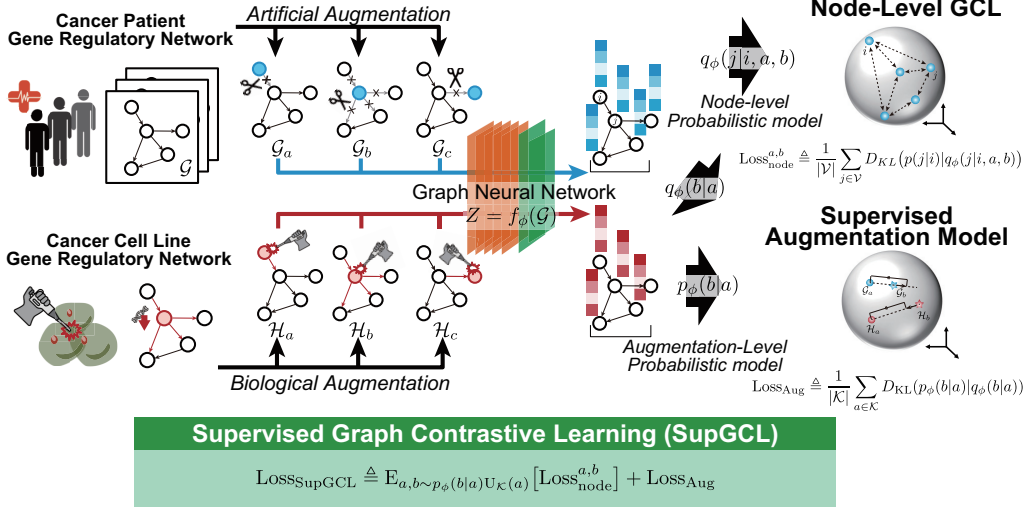


Figure 1: **Schematic overview of SupGCL (Supervised Graph Contrastive Learning)**. The proposed method leverages two complementary types of graph augmentations. First, it generates artificially perturbed GRNs by simulating gene knockdowns, where node and edge features are masked based on the targeted gene. Second, it incorporates biologically grounded augmentations derived from real gene knockdown experiments conducted on cancer cell lines, serving as teacher GRNs. Embeddings are extracted using a shared GNN, and both node-level and augmentation-level contrastive losses are computed using KL divergence. This biologically grounded contrastive framework enables more faithful and effective representation learning of GRNs.

product as the similarity in the matrix space, we define the probability models for the augmentation operations as:

$$p_\phi(b|a) \triangleq \frac{\exp(\text{sim}_F(Y^a, Y^b)/\tau_a)}{\sum_{c \in \mathcal{K}} \exp(\text{sim}_F(Y^a, Y^c)/\tau_a)}, \quad q_\phi(b|a) \triangleq \frac{\exp(\text{sim}_F(Z^a, Z^b)/\tau_a)}{\sum_{c \in \mathcal{K}} \exp(\text{sim}_F(Z^a, Z^c)/\tau_a)}, \quad (6)$$

where $\text{sim}_F(\cdot, \cdot)$ denotes the Frobenius inner product, and $\tau_a > 0$ is a temperature parameter. Unlike node-level learning, $p_\phi(b|a)$ is not a fixed constant but rather a reference distribution based on the supervised embeddings $\{Y^a\}_{a \in \mathcal{K}}$. Both probability models p_ϕ and q_ϕ are parameterized by the same GNN f_ϕ .

Using these probability distributions, substituting the reference model $p_\phi(b|a)$ and the target model $q_\phi(b|a)$ into the formulation of contrastive learning in (1) yields the loss function for augmentation operations:

$$\text{Loss}_{\text{Aug}} \triangleq \frac{1}{|\mathcal{K}|} \sum_{a \in \mathcal{K}} D_{\text{KL}}(p_\phi(b|a) | q_\phi(b|a)). \quad (7)$$

Minimizing this loss reduces the discrepancy in embedding distributions between the artificially augmented graphs and the biologically grounded knockdown graphs. However, if both p_ϕ and q_ϕ are optimized simultaneously, the model may converge to a trivial solution. For instance, if the GNN outputs constant embeddings, both distributions become uniform and $\text{Loss}_{\text{Aug}} = 0$. Thus, minimizing Loss_{Aug} alone is insufficient for learning meaningful graph representations.

To address this issue, here we first introduce a reference model $p_\phi(j, b|i, a)$ and a target model $q_\phi(j, b|i, a)$ that use conditional probabilities for each pair of node and augmentation $(i, a), (j, b) \in \mathcal{V} \times \mathcal{K}$. By substituting these into the contrastive learning formulation in (1), we derive the loss function of Supervised Graph Contrastive Learning:

$$\text{Loss}_{\text{SupGCL}} \triangleq \frac{1}{|\mathcal{V}| |\mathcal{K}|} \sum_{i \in \mathcal{V}, a \in \mathcal{K}} D_{\text{KL}}(p_\phi(j, b|i, a) | q_\phi(j, b|i, a)). \quad (8)$$

Furthermore, the following theorem shows that by assuming independence between nodes and augmentation operations in the reference distribution p_ϕ , we can avoid the trivial solution:

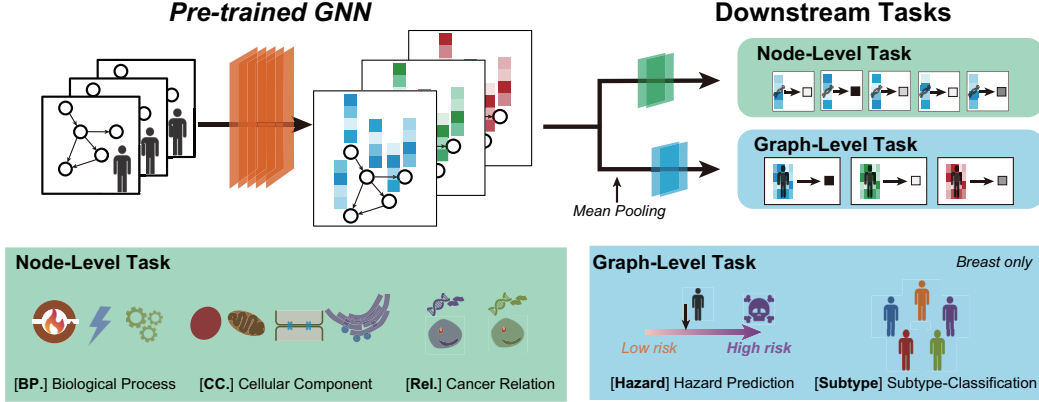


Figure 2: **Overview of Downstream Tasks Used for Benchmark of GRNs Across Three Cancer Types: Breast, Lung, and Colorectal Cancers.** The node-level tasks involve classifying genes into functional categories such as Biological Process [BP.], Cellular Component [CC.], and cancer relevance [Rel.]. The graph-level tasks include patient-level survival risk prediction [Hazard] and disease subtype classification [Subtype], the latter being specific to breast cancer. Mean pooling is applied to obtain graph-level representations.

Theorem 1. Assuming $p_\phi(i, j, a, b) = p(i, j)p_\phi(a, b)$, then

$$\text{LOSS}_{\text{SupGCL}} = \mathbb{E}_{a, b \sim p_\phi(b|a)U_{\mathcal{K}}(a)} [\text{LOSS}_{\text{node}}^{a, b}] + \text{LOSS}_{\text{Aug}}. \quad (9)$$

Proof: This follows directly from the standard decomposition of KL divergence: $D_{\text{KL}}(p(x, y)|q(x, y)) = \mathbb{E}_{x \sim p(x)} [D_{\text{KL}}(p(y|x)|q(y|x))] + D_{\text{KL}}(p(x)|q(x))$. See Appendix A for details. \square

The first term in Theorem 1 corresponds to the expectation of the node-level GCL loss $\text{LOSS}_{\text{node}}^{a, b}$ (as defined in Equation 3) with respect to the supervised augmentation distribution $p_\phi(b|a)$. This allows node-level contrastive learning to reflect biological similarity between knockdown operations. Importantly, since the theorem is independent of the specific choice of the node-level model ($p, q_\phi^{a, b}$), any contrastive loss described by KL divergence can be used in practice. Meanwhile, the second term reduces the distributional difference between the artificially generated augmentation-based GRN and the teacher GRN. Together, these two components ensure both expressive node representations and biologically meaningful augmentations.

Moreover, the performance of node-level representation learning and the biological validity following the teacher data for augmentation operations can be controlled by the temperature parameters τ_n, τ_a of each probability model. In particular, when the temperature parameter τ_a involved in the augmentation operation is sufficiently large, the augmentation operation becomes independent of the teacher GRNs $\{Y_a\}_{a \in \mathcal{K}}$, and coincides with the conventional node-level GCL loss function.

Corollary 1. $\lim_{\tau_a \rightarrow \infty} \text{LOSS}_{\text{SupGCL}} = \text{LOSS}_{\text{node}}$.

Proof: As $\tau_a \rightarrow \infty$, we have $p_\phi(b|a) \rightarrow U_{\mathcal{K}}(b)$ and $q_\phi(b|a) \rightarrow U_{\mathcal{K}}(b)$. Therefore, the expectation term becomes: $\lim_{\tau_a \rightarrow \infty} \mathbb{E}_{a, b \sim p_\phi(b|a)U_{\mathcal{K}}(a)} [\text{LOSS}_{\text{node}}^{a, b}] = \mathbb{E}_{a, b \sim U_{\mathcal{K}}} [\text{LOSS}_{\text{node}}^{a, b}]$, $\lim_{\tau_a \rightarrow \infty} D_{\text{KL}}(p_\phi(b|a)|q_\phi(b|a)) = 0$ thus proving the corollary. \square

In this study, we train the GNN using standard gradient-based optimization applied to the loss function defined in Theorem 1. The corresponding pseudocode is provided in Appendix B.

5 Experiments

In this study, we formulated SupGCL by naturally extending the loss function of conventional GCL, based on a contrastive learning framework using KL divergence. Furthermore, we clarified the

Table 1: Description of downstream task

Task	Task Type	Metrics
Node-Level Task		
[BP.]: Biological process classification	Multi-label binary classification (with 3 labels)	Subset accuracy
[CC.]: Cellular component classification	Multi-label binary classification (with 4 labels)	Subset accuracy
[Rel.]: Cancer relation	Classification (binary)	Accuracy
Graph-Level Task		
[Hazard]: Hazard prediction	Survival analysis (1-dim risk score)	C-index
[Subtype]: Disease subtype prediction	Classification (5 groups)	Subtype accuracy

Table 2: Finetuning result of node-level downstream task.

Task	w/o-pretrain	GAE	GraphCL	GRACE	SGRL	SupGCL
BP.						
Breast	<u>0.232±0.031</u>	0.230±0.029	0.167±0.042	0.230±0.051	0.220±0.052	0.243±0.052
Lung	<u>0.259±0.056</u>	0.247±0.038	0.115±0.024	0.259±0.063	0.233±0.027	0.282±0.037
Colorectal	<u>0.231±0.062</u>	0.245±0.023	0.207±0.058	<u>0.249±0.050</u>	0.146±0.029	0.262±0.030
CC.						
Breast	<u>0.264±0.042</u>	0.250±0.034	0.131±0.050	0.236±0.026	0.249±0.030	0.291±0.026
Lung	<u>0.267±0.041</u>	0.245±0.033	0.069±0.041	0.255±0.043	0.248±0.037	0.274±0.044
Colorectal	<u>0.278±0.098</u>	0.256±0.042	0.190±0.062	0.265±0.030	0.133±0.081	0.279±0.052
Rel.						
Breast	0.573±0.033	0.561±0.059	0.553±0.051	0.575±0.035	<u>0.580±0.055</u>	0.600±0.057
Lung	0.575±0.053	0.568±0.029	0.555±0.036	0.592±0.038	<u>0.593±0.034</u>	0.604±0.053
Colorectal	0.563±0.071	0.574±0.049	0.535±0.056	0.576±0.071	<u>0.580±0.042</u>	0.594±0.039

relationship between SupGCL and conventional GCL through the temperature parameter. This chapter verifies the effectiveness of the proposed method using actual gene regulatory networks (GRNs) from cancer patients and augmented GRNs based on gene knockdown experiments.

5.1 Benchmark of Gene Regulatory Networks

Evaluation Protocol: We evaluated the proposed method through the following procedure. First, based on gene expression data from cancer patients, we constructed patient-specific GRNs. Similarly, we constructed teacher GRNs using gene knockdown experiment data. Then, pre-training was performed on the proposed method using both the patient-specific and teacher GRNs. Subsequently, the performance of the downstream tasks, such as classification accuracy and regression performance, was evaluated using the pre-trained models and compared against comparative methods. Finally, we visualized the latent representations at both the node and graph levels extracted from the trained models.

We compared the proposed method with the following five comparative models:

w/o-pretrain : Directly performs classification or regression for downstream tasks without any pre-training.

GAE : [19]: Graph representation learning method based solely on graph reconstruction.

GraphCL : [13]: Graph contrastive learning using positive pairs between graphs.

GRACE : [15]: Node-level graph contrastive learning method.

SGRL : [17]: Node-level GCL that leverages representation scattering in the embedding space.

Datasets: To evaluate the performance of SupGCL, we conducted benchmark evaluations using real-world datasets. For constructing patient-specific GRNs, we used cancer cell sample data from The Cancer Genome Atlas (TCGA). For constructing teacher GRNs, we used gene knockdown experiment data from cancer cell lines in the Library of Integrated Network-based Cellular Signatures (LINCS). The TCGA dataset [20] and the LINCS dataset [21] are both large-scale and widely-used public platforms providing gene expression data from cancer patients and cell lines, respectively.

Table 3: Finetuning result of graph-level downstream task.

Task	w/o-pretrain	GAE	GraphCL	GRACE	SGRL	SupGCL
Hazard						
Breast	0.601±0.035	0.625±0.035	0.638±0.049	<u>0.642±0.064</u>	0.640±0.077	0.650±0.059
Lung	0.611±0.052	<u>0.619±0.062</u>	0.616±0.049	0.609±0.055	0.611±0.060	0.627±0.051
Colorectal	0.621±0.070	0.631±0.091	<u>0.657±0.071</u>	0.647±0.059	0.616±0.123	0.698±0.085
Subtype						
Breast	0.804±0.031	0.834±0.028	0.719±0.077	<u>0.841±0.026</u>	0.829±0.030	0.847±0.036

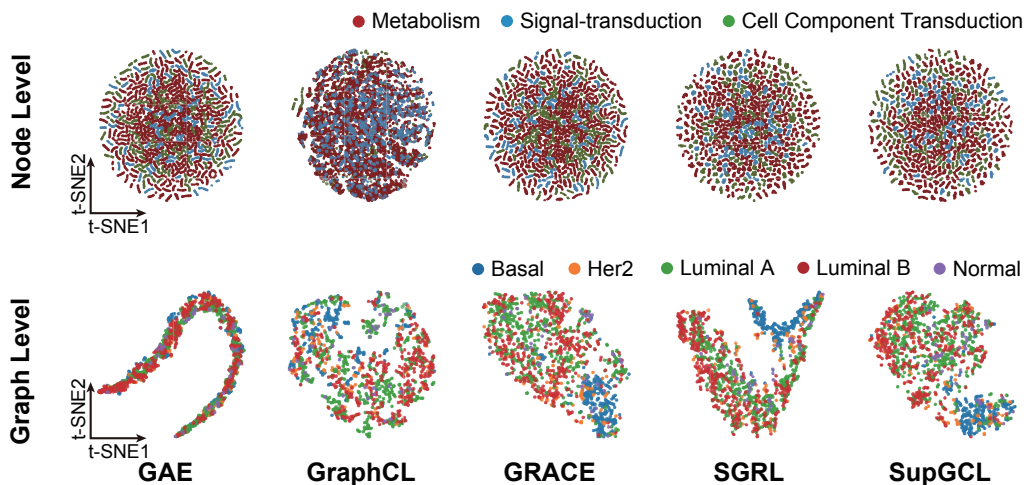


Figure 3: t-SNE visualization of pre-trained embeddings on breast cancer GRNs. The top row shows the node-level embedding space for individual genes, and the bottom row shows the corresponding graph-level readout features for each patient’s network.

We used normalized count data from the TCGA TARGET GTEx study [22] provided by UCSC Xena. For LINCS, we used normalized gene expression data from the LINCS L1000 GEO dataset (GSE92742) [23].

Experiments were conducted for three cancer types across both datasets: breast cancer, lung cancer, and colorectal cancer. Furthermore, the set of genes constituting each network was restricted to the 975 genes common to the TCGA gene set and the 978 LINCS landmark genes. The number of patient samples for each cancer type was $N=1092$ (breast), 1011 (lung), and 288 (colorectal), and the total number of knockdown experiments was 8793, 11843, and 15926, respectively. The number of unique knockdown target genes / total common genes was 768/975, 948/975, and 948/975.

The TCGA dataset also includes survival status and disease subtype labels associated with each gene expression profile. Additionally, each gene was annotated with multi-labels based on Gene Ontology [24] — Biological Process (metabolism, signaling, cell organization; 3 classes), and Cellular Component (nucleus, mitochondria, ER, membrane; 4 classes). We also used the OncoKB [25] cancer-related gene list to assign binary relevance labels. These labels were used for downstream tasks. Details are provided in Appendix C.

Pre-processing: To estimate the network structure of each GRN from gene expression data, we used a Bayesian network structure learning algorithm based on nonparametric regression with Gaussian noise [26]. For each experiment, gene expression values were used as node features, while edge features were defined as the product of estimated regression coefficients and the parent node’s gene expression [27]. This structure estimation was performed per cancer type per dataset using the above algorithm. Further details are provided in Appendix D.

5.2 Result 1: Evaluation by Downstream Task

In this experiment, pre-training of the proposed and conventional methods was conducted using patient-specific GRNs from TCGA and teacher GRNs from LINCS. Subsequently, fine-tuning was performed on the pre-trained models using patient GRNs, and downstream task performance was evaluated (see Figure 2). During fine-tuning, two additional fully connected layers were appended to the node-level representations and graph-level representations (obtained via mean pooling), and downstream tasks were performed.

Graph-level tasks (hazard prediction, subtype classification) used survival and subtype labels from TCGA. Note that subtype classification was conducted only for breast cancer. Node-level tasks (Biological Process - BP, Cellular Component - CC, and cancer relevance - Rel.) used gene-level annotations from Gene Ontology and OncoKB.

Details of these downstream tasks are summarized in Table 1.

Each downstream task — hazard prediction, subtype classification, BP, and CC classification — was evaluated using 10-fold cross-validation. For cancer gene classification, due to label imbalance, we performed undersampling over 10 random seeds. Results are reported as mean \pm standard deviation.

For all methods including the SupGCL and conventional methods, we used the same 5-layer Graph Transformer architecture [28]. Hyperparameters for pre-training were tuned with Optuna [29], and the model was optimized using the AdamW optimizer [30]. All training runs were performed on a single NVIDIA H100 SXM5 GPU. Additional experimental details can be found in Appendix E.

Tables 2 and 3 show the results for node-level and graph-level tasks, respectively. The best performance is indicated in bold, and the second-best is underlined. Although SupGCL did not achieve statistically significant superiority in every single task, it consistently outperformed other pre-training methods across all datasets and tasks.

For node-level tasks, many existing methods did not show much improvement over without-pretrain, whereas SupGCL consistently demonstrated strong performance. This suggests that SupGCL effectively captures biologically meaningful GRN representations suitable for these tasks. In graph-level tasks like hazard and subtype prediction, while some existing methods showed marginal improvement over without-pretrain, SupGCL achieved significantly higher performance.

5.3 Result 2: Latent Space Analysis

Using the pre-trained models, we visualized the embedding spaces derived from the breast cancer dataset (see Figure 3). Other similar visualizations are shown in Appendix F.

The top row of Figure 3 shows the node-level embeddings. Colors represent one of the three single-label Biological Process annotations (metabolism, signaling, or cell organization). Across all models, no clear clustering was observed based on labels. However, GraphCL’s embeddings were notably different from others, with signs of latent space collapse. Detailed observations are provided in Appendix F. This suggests that GraphCL may be more suited to graph-level discrimination than node-level representation.

Compared to GraphCL, the other models showed more dispersed embeddings, though without distinct clustering.

The bottom row of Figure 3 illustrates the graph-level embeddings, colored by disease subtype. From this, it is evident that GAE and GraphCL fail to separate subtypes in the embedding space. In contrast, GRACE and SGRL showed moderate separation between the Basal subtype and others. SupGCL displayed the clearest separation, indicating its ability to better learn subtype-specific network representations.

6 Conclusion

In this study, we proposed a supervised graph contrastive learning method, SupGCL, for representation learning of gene regulatory networks (GRNs), which incorporates real-world genetic perturbation data as supervision during training. We formulated GCL with supervision-guided augmentation selection within a unified probabilistic framework, and theoretically demonstrated that conventional

GCL methods are special cases of our proposed formulation. Through benchmark evaluations using downstream tasks based on both node-level and graph-level embeddings of GRNs from cancer patients, SupGCL consistently outperformed existing GCL methods.

A limitation of this paper is that the effectiveness of the proposed method has only been confirmed in situations where the teacher GRNs were constructed from knockdown experiments of the same cancer type.

As future work, we plan to expand the target cancer types and develop a large-scale, general-purpose SupGCL model that can operate across multiple cancer types.

Acknowledgments and Disclosure of Funding

This work was supported by JST Moonshot R&D Grant Number JPMJMS2021, JPMJMS2024, and JSPS KAKENHI Grant Number 25K00148. This work used computational resources of the supercomputer Fugaku provided by RIKEN through the HPCI System Research Project (Project IDs: hp150272, ra000018).

References

- [1] Wei Ju, Zheng Fang, Yiyang Gu, Zequn Liu, Qingqing Long, Ziyue Qiao, Yifang Qin, Jianhao Shen, Fang Sun, Zhiping Xiao, Junwei Yang, Jingyang Yuan, Yusheng Zhao, Yifan Wang, Xiao Luo, and Ming Zhang. A comprehensive survey on deep graph representation learning. *Neural Networks*, 173:106207, May 2024.
- [2] Xinxin Hu, Haotian Chen, Hongchang Chen, Shuxin Liu, Xing Li, Shibo Zhang, Yahui Wang, and Xiangyang Xue. Cost-sensitive gnn-based imbalanced learning for mobile social network fraud detection. *IEEE Transactions on Computational Social Systems*, 11(2):2675–2690, 2023.
- [3] Xintao Shen and Yulai Zhang. A knowledge graph recommendation approach incorporating contrastive and relationship learning. *IEEE Access*, 11:99628–99637, 2023.
- [4] Tianyu Liu, Yuge Wang, Rex Ying, and Hongyu Zhao. Muse-gnn: Learning unified gene representation from multimodal biological graph data. *Advances in neural information processing systems*, 36:24661–24677, 2023.
- [5] Lirong Wu, Haitao Lin, Cheng Tan, Zhangyang Gao, and Stan Z Li. Self-supervised learning on graphs: Contrastive, generative, or predictive. *IEEE Transactions on Knowledge and Data Engineering*, 35(4):4216–4235, 2021.
- [6] Weiming Yu, Zerun Lin, Miaofang Lan, and Le Ou-Yang. Gclink: a graph contrastive link prediction framework for gene regulatory network inference. *Bioinformatics*, 41(3):btaf074, 2025.
- [7] Xuan Liu, Congzhi Song, Feng Huang, Haitao Fu, Wenjie Xiao, and Wen Zhang. Graphcdr: a graph neural network method with contrastive learning for cancer drug response prediction. *Briefings in Bioinformatics*, 23(1):bbab457, 2022.
- [8] Mai Adachi Nakazawa, Yoshinori Tamada, Yoshihisa Tanaka, Marie Ikeguchi, Kako Higashihara, and Yasushi Okuno. Novel cancer subtyping method based on patient-specific gene regulatory network. *Scientific reports*, 11(1):23653, 2021.
- [9] Yuning You, Tianlong Chen, Yongduo Sui, Ting Chen, Zhangyang Wang, and Yang Shen. Graph contrastive learning with augmentations. *Advances in neural information processing systems*, 33:5812–5823, 2020.
- [10] Yanqiao Zhu, Yichen Xu, Feng Yu, Qiang Liu, Shu Wu, and Liang Wang. Graph contrastive learning with adaptive augmentation. In *Proceedings of the web conference 2021*, pages 2069–2080, 2021.
- [11] Chenhao Wang, Yong Liu, Yan Yang, and Wei Li. Hetergcl: graph contrastive learning framework on heterophilic graph. In *Proceedings of the Thirty-Third International Joint Conference on Artificial Intelligence*, pages 2397–2405, 2024.
- [12] Evan O Paull, Alvaro Aytes, Sunny J Jones, Prem S Subramaniam, Federico M Giorgi, Eugene F Douglass, Somnath Tagore, Brennan Chu, Alessandro Vasciaveo, Siyuan Zheng, et al. A modular master regulator landscape controls cancer transcriptional identity. *Cell*, 184(2):334–351, 2021.
- [13] Yuning You, Tianlong Chen, Yang Shen, and Zhangyang Wang. Graph contrastive learning automated. In *International conference on machine learning*, pages 12121–12132. PMLR, 2021.

- [14] Jiawei Sun, Ruoxin Chen, Jie Li, Yue Ding, Chentao Wu, Zhi Liu, and Junchi Yan. Understanding and mitigating dimensional collapse of graph contrastive learning: A non-maximum removal approach. *Neural Networks*, 181:106652, 2025.
- [15] Yanqiao Zhu, Yichen Xu, Feng Yu, Qiang Liu, Shu Wu, and Liang Wang. Deep graph contrastive representation learning. *arXiv preprint arXiv:2006.04131*, 2020.
- [16] Shantanu Thakoor, Corentin Tallec, Mohammad Gheshlaghi Azar, Rémi Munos, Petar Veličković, and Michal Valko. Bootstrapped representation learning on graphs. In *ICLR 2021 workshop on geometrical and topological representation learning*, 2021.
- [17] Dongxiao He, Lianze Shan, Jitao Zhao, Hengrui Zhang, Zhen Wang, and Weixiong Zhang. Exploitation of a latent mechanism in graph contrastive learning: Representation scattering. *Advances in Neural Information Processing Systems*, 37:115351–115376, 2024.
- [18] Shaden Alshammari, John Hershey, Axel Feldmann, William T Freeman, and Mark Hamilton. I-con: A unifying framework for representation learning. *arXiv preprint arXiv:2504.16929*, 2025.
- [19] Thomas N Kipf and Max Welling. Variational graph auto-encoders. *arXiv preprint arXiv:1611.07308*, 2016.
- [20] John N Weinstein, Eric A Collisson, Gordon B Mills, Karthik R M Shaw, Bradley A Ozenberger, Kyle Ellrott, Ilya Shmulevich, Chris Sander, Joshua M Stuart, et al. The cancer genome atlas pan-cancer analysis project. *Nature Genetics*, 45(10):1113–1120, 2013.
- [21] Aravind Subramanian, Ramachandran Narayan, Simone M Corsello, and et al. A next generation connectivity map: L1000 platform and the first 1,000,000 profiles. *Cell*, 171(6):1437–1452.e17, 2017.
- [22] UCSC Xena. TCGA TARGET GTEx study data. Available from UCSC Xena Platform, 2016. Accessed: 2025-05-15.
- [23] Subramanian. GEO: Gene Expression Omnibus, GSE92742: L1000 phase I landmark gene expression profiles, 2017. Accessed: 2025-05-15.
- [24] Michael Ashburner, Catherine A Ball, Judith A Blake, David Botstein, Helen Butler, J Michael Cherry, Ana Davis, Kara Dolinski, Sally S Dwight, Janan T Eppig, et al. Gene ontology: tool for the unification of biology. *Nature Genetics*, 25(1):25–29, 2000.
- [25] Debyani Chakravarty, J Gao, S Phillips, R Kundra, H Zhang, J Wang, J E Rudolph, R Yaeger, T Soumerai, M Nissan, et al. Oncokb: A precision oncology knowledge base. *JCO Precision Oncology*, 2017:PO.17.00011, 2017.
- [26] Seiya Imoto, Takao Goto, and Satoru Miyano. Estimation of genetic networks and functional structures between genes by using Bayesian networks and nonparametric regression. *Pacific Symposium on Biocomputing. Pacific Symposium on Biocomputing*, pages 175–186, 2002.
- [27] Yoshihisa Tanaka, Yoshinori Tamada, Marie Ikeguchi, Fumiyoshi Yamashita, and Yasushi Okuno. System-based differential gene network analysis for characterizing a sample-specific subnetwork. *Biomolecules*, 10(2), 2020.
- [28] Yunsheng Shi, Zhengjie Huang, Shikun Feng, Hui Zhong, Wenjin Wang, and Yu Sun. Masked label prediction: Unified message passing model for semi-supervised classification. *arXiv preprint arXiv:2009.03509*, 2020.
- [29] Takuya Akiba, Shotaro Sano, Tetsuo Yanase, Toshihiko Ohta, and Masanori Koyama. Optuna: A next-generation hyperparameter optimization framework. In *Proceedings of the 25th ACM SIGKDD International Conference on Knowledge Discovery & Data Mining (KDD '19)*, pages 2623–2631, Anchorage, AK, USA, 2019. ACM.
- [30] Ilya Loshchilov and Frank Hutter. Decoupled weight decay regularization. *International Conference on Learning Representations (ICLR)*, 2019.
- [31] Anna R Paolacci, Oronzo A Tanzarella, Enrico Porceddu, and Mario Ciaffi. Identification and validation of reference genes for quantitative rt-pcr normalization in wheat. *BMC molecular biology*, 10:1–27, 2009.
- [32] Pedro R Costa, Marcio L Acencio, and Ney Lemke. A machine learning approach for genome-wide prediction of morbid and druggable human genes based on systems-level data. In *BMC genomics*, volume 11, pages 1–15. Springer, 2010.

- [33] Jiwen Xin, Adam Mark, Cyrus Afrasiabi, Ginger Tsueng, Moritz Juchler, Nikhil Gopal, Gregory S Stupp, Timothy E Putman, Benjamin J Ainscough, Obi L Griffith, et al. Mygene. info and myvariant. info: gene and variant annotation query services. *bioRxiv*, page 035667, 2015.
- [34] Michael Ashburner, Catherine A Ball, Judith A Blake, David Botstein, Heather Butler, J Michael Cherry, Allan P Davis, Kara Dolinski, Selina S Dwight, Janan T Eppig, et al. Gene ontology: tool for the unification of biology. *Nature genetics*, 25(1):25–29, 2000.
- [35] Peter Langfelder and Steve Horvath. WGCNA: an R package for weighted correlation network analysis. *BMC Bioinformatics*, 9(1):559, December 2008.
- [36] Adam A. Margolin, Ilya Nemenman, Katia Basso, Chris Wiggins, Gustavo Stolovitzky, Riccardo Dalla Favera, and Andrea Califano. ARACNE: An Algorithm for the Reconstruction of Gene Regulatory Networks in a Mammalian Cellular Context. *BMC Bioinformatics*, 7(1):S7, March 2006.
- [37] Nir Friedman, Michal Linial, Iftach Nachman, and Dana Pe’er. Using Bayesian networks to analyze expression data. In *Proceedings of the fourth annual international conference on Computational molecular biology*, RECOMB ’00, pages 127–135, New York, NY, USA, 2000. Association for Computing Machinery.
- [38] Hantao Shu, Jingtian Zhou, Qiuyu Lian, Han Li, Dan Zhao, Jianyang Zeng, and Jianzhu Ma. Modeling gene regulatory networks using neural network architectures. *Nature Computational Science*, 1(7):491–501, July 2021. Publisher: Nature Publishing Group.
- [39] Seiya Imoto, Sunyong Kim, Takao Goto, Sachiyo Aburatani, Kousuke Tashiro, Satoru Kuhara, and Satoru Miyano. Bayesian network and nonparametric heteroscedastic regression for nonlinear modeling of genetic network. *Journal of bioinformatics and computational biology*, 1(02):231–252, 2003.
- [40] Mei Tomoto, Yohei Mineharu, Noriaki Sato, Yoshinori Tamada, Mari Nogami-Itoh, Masataka Kuroda, Jun Adachi, Yoshito Takeda, Kenji Mizuguchi, Atsushi Kumanogoh, Yayoi Natsume-Kitatani, and Yasushi Okuno. Idiopathic pulmonary fibrosis-specific Bayesian network integrating extracellular vesicle proteome and clinical information. *Scientific Reports*, 14(1):1315, January 2024. Publisher: Nature Publishing Group.
- [41] Hiroko Yahara, Souichi Yanamoto, Miho Takahashi, Yuji Hamada, Haruo Sakamoto, Takuya Asaka, Yoshimasa Kitagawa, Kuniyasu Moridera, Kazuma Noguchi, Masaya Sugiyama, Yutaka Maruoka, and Koji Yahara. Whole blood transcriptome profiling identifies gene expression subnetworks and a key gene characteristic of the rare type of osteomyelitis. *Biochemistry and Biophysics Reports*, 32:101328, December 2022.
- [42] Yoshinori Tamada, Teppei Shimamura, Rui Yamaguchi, Seiya Imoto, Masao Nagasaki, and Satoru Miyano. Sign: Large-Scale Gene Network Estimation Environment for High Performance Computing. *Genome Informatics*, 25(1):40–52, 2011.

A Detail Proof of Theorem 1

Since the loss function of contrastive learning (1) is fomulated as the KL divergence between the joint distributions $p(x, y)$ and $q(x, y)$, under the assumption that $p(x)$ and $q(x)$ follow uniform distributions. Then, the following derived for $\text{Loss}_{\text{I-CON}}$:

$$\begin{aligned}
\text{Loss}_{\text{SupGCL}} &= \frac{1}{|V||\mathcal{K}|} \sum_{i \in V, a \in \mathcal{K}} D_{\text{KL}}(p_\phi(j, b|i, a)|q_\phi(j, b|i, a)). \\
&= D_{\text{KL}}(p_\phi(i, j, a, b)|q_\phi(i, j, a, b)) \\
&= \mathbb{E}_{(a,b) \sim p_\phi(a,b)} \left[D_{\text{KL}}(p_\phi(i, j|a, b)|q_\phi(i, j|a, b)) \right] + D_{\text{KL}}(p_\phi(a, b)|q_\phi(a, b)) \\
&= \mathbb{E}_{(a,b) \sim p_\phi(a,b)} \left[D_{\text{KL}}(p(i, j)|q_\phi(i, j|a, b)) \right] + D_{\text{KL}}(p_\phi(a, b)|q_\phi(a, b)) \\
&= \mathbb{E}_{a,b \sim p_\phi(b|a) \cup_{\mathcal{K}}(a)} [\text{Loss}_{\text{node}}^{a,b}] + \text{Loss}_{\text{Aug}}
\end{aligned}$$

The derivation from the second to the third line utilizes the basic decomposition of KL divergence: $D_{\text{KL}}(p(x, y)|q(x, y)) = \mathbb{E}_{x \sim p(x)} [D_{\text{KL}}(p(y|x)|q(y|x))] + D_{\text{KL}}(p(x)|q(x))$.

B Algorithm

The learning algorithm of this research is presented in Algorithm 1. We train the Graph Neural Network (GNN) f_ϕ using the target GRN dataset for all patients, $\mathcal{G}_{\text{all}} = \{\mathcal{G}^{(i)}\}_{i=1}^N$, and the teacher GRN dataset, $\mathcal{H}_{\text{all}} = \{\mathcal{H}_a^{(i)}\}_{i \in \mathcal{I}_a, a \in \mathcal{K}}$. Here, \mathcal{I}_a is the set of indices for teacher GRNs, $\{\mathcal{H}_a^{(i)}\}_{i \in \mathcal{I}_a}$, which correspond to data augmentations for the a -th node.

Our algorithm follows a standard training loop, consisting of the calculation of $\text{Loss}_{\text{SupGCL}}$ and the optimization of f_ϕ using AdamW. Furthermore, to reduce computational costs, we employ sampling-based estimation of the normalization constant for the calculation of softmax functions $p_\phi(b|a)$ and $q_\phi(b|a)$, and use importance sampling for the calculation of $\text{Loss}_{\text{node}}^{a,b}$ and Loss_{Aug} .

Algorithm 1 Training loop of SupGCL:

Require: Graph Neural Net f_ϕ , all patient GRNs $\mathcal{G}_{\text{all}} = \{\mathcal{G}^{(i)}\}_{i=1}^N$, all teacher GRNs $\mathcal{H}_{\text{all}} = \{\mathcal{H}_a^{(i)}\}_{i \in \mathcal{I}_a, a \in \mathcal{K}}$

- 1: **for** $\mathcal{G} \subset \mathcal{G}_{\text{all}}$ **do**
- 2: $a, b \sim \mathbb{U}_{\mathcal{K}}$
- 3: $\mathcal{G}_a, \mathcal{G}_b \leftarrow$ The a -th and b -th artificial augmentation of \mathcal{G}
- 4: $\mathcal{H}_a, \mathcal{H}_b \leftarrow$ Pick up the a -th and b -th knockdown teacher GRN from \mathcal{H}_{all}
- 5: $Z^a, Z^b \leftarrow f_\phi(\mathcal{G}_a), f_\phi(\mathcal{G}_b)$ ▷ Embedding target GRNs
- 6: $Y^a, Y^b \leftarrow f_\phi(\mathcal{H}_a), f_\phi(\mathcal{H}_b)$ ▷ Embedding teacher GRNs
- 7: $q_\phi(b|a) \leftarrow \text{softmax} \left(\left[\frac{\langle Z^a, Z^* \rangle_F}{\tau_a} \right] \right) [b]$ ▷ Calculate augmentation-level target model
- 8: $p_\phi(b|a) \leftarrow \text{softmax} \left(\left[\frac{\langle Y^a, Y^* \rangle_F}{\tau_a} \right] \right) [b]$ ▷ Calculate augmentation-level teacher model
- 9: $\text{Loss}_{\text{Aug}} \leftarrow |\mathcal{K}| p_\phi(b|a) (\log p_\phi(b|a) - \log q_\phi(b|a))$ ▷ Importance sampling of $\text{Loss}_{\text{Aug}}^{a,b}$
- 10: $q_\phi(j|i, a, b) \leftarrow \text{softmax} \left(\left[\frac{\langle z_i^a, z_*^b \rangle}{\tau_n} \right] \right) [j]$ ▷ Calculate node-level target model
- 11: $\text{Loss}_{\text{node}}^{a,b} \leftarrow \frac{1}{|V|} \sum_{i \in V} \log q_\phi(i|i, a, b)$
- 12: $\text{Loss}_{\text{SupGCL}} \leftarrow |\mathcal{K}| p_\phi(b|a) \text{Loss}_{\text{node}}^{a,b} + \text{Loss}_{\text{Aug}}$ ▷ Importance sampling of $\text{Loss}_{\text{node}}^{a,b}$
- 13: Update f_ϕ using $\text{Loss}_{\text{SupGCL}}$ and AdamW optimizer
- 14: **end for**
- 15: **return** Trained Graph NN: f_ϕ

C Details of Experimental Datasets

This section provides details on data acquisition and preprocessing procedures.

C.1 Details on the TCGA Dataset

In this study, we utilized the TCGA TARGET GTEx platform provided by UCSC Xena to extract patient-specific expression data and clinical labels (survival time data, disease subtype labels) for downstream tasks.

The TCGA platform contains four datasets: the gene expression dataset "dataset: gene expression RNAseq – RSEM norm_count," the dataset for cancer type attributes of individual patients "dataset: phenotype – TCGA TARGET GTEx selected phenotypes," the patient prognosis dataset "dataset: phenotype – TCGA survival data," and the patient phenotype data "dataset: phenotype - Phenotypes."

In this study, based on the dataset of patient cancer type attributes, we extracted patient IDs corresponding to the TCGA cohorts listed in Table 4, and subsequently obtained the associated gene expression data. Notably, the study population was limited to patients whose target cancer was a primary tumor. Additionally, overall survival time (OS.time) and survival status (OS: alive = 0 / deceased = 1) were retrieved from the patient prognosis dataset. For breast cancer specifically, disease subtype labels based on the PAM50 classification were acquired from the patient phenotype dataset. PAM50 classification using RNA expression data was feasible for all samples, assigning all 1,092 breast cancer patients to one of five subtypes: Luminal A (N = 438), Luminal B (N = 311), Basal (N = 196), Her2 (N = 111), and Normal (N = 36). Patient samples with missing values were excluded during the data extraction process. The final sample sizes and mortality rates for each cancer type after processing are summarized in Table 4.

Table 4: Sample extraction conditions and survival data statistics for each cancer type

Cancer Type	TCGA Cohort Name	Number of samples with valid survival time data	Number of deaths	Mortality rate (%)
Breast cancer	Breast Invasive Carcinoma	1,090	151	13.9
Lung cancer	Lung Adenocarcinoma + Lung Squamous Cell Carcinoma	996	394	39.6
Colon cancer	Colon Adenocarcinoma	286	69	24.1

C.2 Details on the LINCS Dataset

In this study, we used the Level 3 normalized gene expression data (filename on LINCS datasets: "GSE92742_Broad_LINCS_Level3_INF_mlr12k_n1319138x12328.gctx.gz") provided from the GEO dataset (GSE92742) of the LINCS L1000 project. Additionally, by referring to the concurrently provided experimental metadata ("GSE92742_Broad_LINCS_inst_info.txt.gz" indicating cell lines and treatment conditions, and "GSE92742_Broad_LINCS_pert_info.txt.gz" indicating drug and gene knockdown information), we extracted only the shRNA-mediated knockdown experiment groups. The cell lines and treatment durations were limited to samples from: MCF7 breast cancer cell line treated for 96 hours, A549 lung cancer cell line treated for 96 hours, and HT29 colon cancer cell line treated for 96 hours. The expression data was limited to 978 landmark genes.

C.3 Extraction of Gene Label Data for BP/CC Tasks using Gene Ontology

In this study, for Biological Process (BP) classification and Cellular Component (CC) classification in downstream tasks, we performed multi-label annotation for each of the 975 genes constituting the GRN, based on terms obtained from the GO database. For BP labels, three categories whose importance is known were used: 'Metabolism', 'Signal Transduction', and 'Cellular Organization' [31]. Similarly, for CC labels, four categories were used: 'Nucleus', 'Mitochondrion', 'Endoplasmic Reticulum', and 'Plasma Membrane' [32]. These categories were selected to cover the major functions of the GRN.

To extract these multi-labels, the following steps were performed:

1. Batch retrieve terms associated with each gene using the MyGene.info API [33] and the OBO file (available at <https://geneontology.org/docs/download-ontology/>).
2. Aggregate multi-labels for the target genes using the GOOtools library [34].

Genes that could not be labeled into any of the BP or CC categories were excluded from the downstream tasks in this study. The number and percentage of genes included in each category are shown in Table 5.

Table 5: Gene label distribution for high-level BP/CC categories (n = 975)

Category	Number of genes	Percentage of category (%)
BP: Metabolism	533	54.67
BP: Signal Transduction	261	26.77
BP: Cellular Organization	369	37.85
BP: Not Applicable	204	20.92
CC: Nucleus	388	39.80
CC: Mitochondrion	151	12.49
CC: Endoplasmic Reticulum	148	15.18
CC: Plasma Membrane	231	23.69
CC: Not Applicable	257	26.36

C.3.1 Annotation by OncoKB

For cancer-related gene classification in downstream tasks, cancer-related genes were obtained from the OncoKB™ Cancer Gene List provided by OncoKB (Oncology Knowledge Base) [25]. Using the list of 1188 cancer-related genes provided as of April 30, 2025, positive labels were assigned to the 975 genes used in this study. As a result, 106 genes were labeled as cancer-related genes.

D Estimating Gene Regulatory Networks

D.1 Taxonomy of Gene Regulatory Network Estimation

Estimating accurate gene regulatory networks (GRNs) is crucial for elucidating cellular processes and disease mechanisms. Methods for computationally estimating GRNs from gene expression data can be categorized into correlation-based [35], mutual information-based [36], probabilistic graphical models-based such as Bayesian networks [37], and deep learning-based approaches [38]. The number of experimentally validated GRNs is limited. Therefore, GRN estimation methods need the ability to account for measurement errors and appropriately capture non-linear and multimodal interactions between genes while mitigating overfitting. Thus, we adopted a method combining Bayesian network estimation using multiple sampling and non-parametric regression [26] to identify patient- or sample-specific GRNs [8].

D.1.1 Details of Estimating GRNs

To construct patient-specific GRNs, we estimate Bayesian Networks using B-spline regression. First, we estimate the conditional probability density functions between genes using the entire gene expression dataset. Then, using these learned parameters, we construct patient- or sample-specific GRNs.

Let x_1, x_2, \dots, x_n be random variables for n nodes, and let $\text{pa}(i)$ be the set of parent nodes of the i -th node. In this case, a Bayesian network using B-spline curves [26] is defined as a probabilistic model decomposed into conditional distributions with parent nodes:

$$\begin{aligned}
 p(x_1, \dots, x_n) &= \prod_{i=1}^n p(x_i | x_{\text{pa}(i)}) \\
 &= \prod_{i=1}^n \mathcal{N}\left(x_i \mid \sum_{j \in \text{pa}(i)} m_{ij}(x_j), \sigma^2\right).
 \end{aligned}$$

Here, \mathcal{N} is a Gaussian distribution, and m_{ij} is a B-spline curve defined by B-spline basis functions $b_s : \mathbb{R} \rightarrow \mathbb{R}$ as

$$m_{ij}(x_j) = \sum_{s=1}^M w_{i,j}^s b_s(x_j) \quad (10)$$

The Bayesian network is estimated by learning the relationships with parent nodes based on the model described above and the parameters of the conditional distributions. In this study, the score function used for searching the structure of the Bayesian Network can be analytically derived using Laplace approximation [26]. Since the problem of finding a Directed Acyclic Graph (DAG) that maximizes this score is NP-hard, we performed structure search using a heuristic structure estimation algorithm, the greedy hill-climbing (HC) algorithm [39]. Furthermore, to ensure the reliability of the estimation results by the HC algorithm, we performed multiple sampling runs.

We extracted edges that appeared more frequently than a predefined threshold relative to the number of sampling runs in the estimated networks. Finally, for each edge in the obtained network structure, the conditional probabilities were relearned using all input data.

Using the network and conditional probabilities learned here, we derive patient-specific GRNs [27]. The node set and edge set of the graph for a patient-specific GRN are defined by the network learned with gene expression levels as random variables x_1, \dots, x_n . Furthermore, the feature of the i -th node X_i^y is the gene expression level of each sample, and the feature of an edge from i to j (designated as the k -th edge) is the realization of the learned B-spline curve $X_k^{\mathcal{E}} = m_{ij}(x_j)$. Patient-specific networks using such edge features have led to the discovery of subtypes that correlate more strongly with prognosis than existing subtypes [8]. Additionally, using differences in edge features between patients to extract patient-specific networks has been reported to contribute to the identification of novel diagnostic and therapeutic marker candidates in diseases such as idiopathic pulmonary fibrosis [40] and chronic nonbacterial osteomyelitis [41]

For GRN estimation, we used INGOR (version 0.19.0), a software that estimates Bayesian Networks based on B-spline regression, and executed it on the supercomputer Fugaku. INGOR is based on SiGN-BN [42], a software that similarly estimates Bayesian Networks using B-spline regression, and achieves faster estimation by optimizing parallel computation on Fugaku. In all GRN estimations, the number of sampling runs was set to 1000, and the threshold for adopting edges was set to 0.05. Since network estimation with a large amount of sample data can lead to Out of Memory errors, the upper limit of gene expression data used for network estimation was set to 3000 (especially for LINCS data). All other hyperparameters related to network estimation used the default settings of SiGN-BN. The number of Fugaku nodes and the required execution times are shown in Table 6. In addition, the number of parallel threads was set to 4 for estimations using TCGA data and 2 for LINCS data.

Table 6: Estimated network times in supercomputer Fugaku

	Breast cancer		Lung cancer		Colorectal cancer	
	TCGA	LINCS	TCGA	LINCS	TCGA	LINCS
Number of Fugaku Nodes	288	288	288	528	288	528
Estimated Time [hh:mm:ss]	00:54:49	08:35:12	00:38:24	13:28:07	00:05:40	21:01:38

D.2 Results

The statistics of the estimated networks are shown in Table 7. It should be noted that network estimation methods using sampling can extract highly reliable edges, but they may occasionally extract structures containing cyclic edges. However, all networks estimated in this study maintained a DAG structure.

Table 7: Estimated network statistics

	Breast cancer		Lung cancer		Colorectal cancer	
	TCGA	LINCS	TCGA	LINCS	TCGA	LINCS
Number of Nodes	975	975	975	975	975	975
Number of Edges	13170	10498	13322	13968	13686	12541
Average Degree	13.5077	10.7671	13.6636	14.3262	14.0369	12.8626

E Experimental Setting

E.1 Hyperparameters Settings

In this study, we used Optuna [29], a Bayesian optimization tool, for hyperparameter search in pre-training. The search space for all models included the AdamW learning rate $lr \in [10^{-5}, 10^{-3}]$, batch size $batch_size \in \{4, 8\}$, and model-specific hyperparameters. Model-specific hyperparameters were the temperature parameter $\tau \in \{0.25, 0.5, 0.75, 1.0\}$ for GraphCL, GRACE, and SupGCL, and the global-hop parameter $k \in \{1, 2, 3\}$ for SGRL. The graph embedding dimension was unified to 64 for all models. See Appendix F for a discussion on embedding dimension. For training the pre-trained models, the data was split into training and validation sets at an 8 : 2 ratio, and the validation loss was used as the metric for various decisions. The optimal hyperparameters determined by actual hyperparameter tuning are shown in Table 8.

Table 8: Hyperparameter settings for each cancer type

Cancer Type	Model	learning rate	batch size	temperature	global hop
Breast cancer	GAE	5.74×10^{-4}	4	—	—
	GRACE	9.71×10^{-4}	4	0.25	—
	GraphCL	1.23×10^{-4}	4	0.25	—
	SGRL	2.39×10^{-4}	4	—	3
	SupGCL	2.37×10^{-4}	4	0.25	—
Lung cancer	GAE	2.16×10^{-4}	4	—	—
	GRACE	4.44×10^{-5}	8	0.25	—
	GraphCL	6.24×10^{-5}	4	0.25	—
	SGRL	8.18×10^{-5}	8	—	2
	SupGCL	1.89×10^{-4}	4	0.25	—
Colorectal cancer	GAE	2.26×10^{-4}	4	—	—
	GRACE	4.03×10^{-5}	8	0.25	—
	GraphCL	8.83×10^{-5}	4	0.25	—
	SGRL	7.10×10^{-4}	4	—	3
	SupGCL	3.32×10^{-4}	4	0.25	—

E.2 Computational Environment and Computation Time

All experiments were conducted on an NVIDIA H100 SXM5 (95.83 GiB), and the computation time for each model is shown in Table 9. Please note that although the number of training steps is based on 3000 epochs, the actual training time varies due to early stopping using the validation data.

E.3 Fine-tuning Settings

E.3.1 Graph-Level Task

For fine-tuning graph-level tasks (Hazard Prediction, Subtype Classification), training was performed on a per-patient basis. The latent states embedded by the Graph Neural Network were transformed into graph-level embeddings using mean-pooling, and then fed through a 2-layer MLP to train task-specific models.

Table 9: Pre-training computation time for each cancer type

Cancer Type	Model	Computation Time	Epochs
Breast cancer	GAE	3.354 hr	3000
	GRACE	10.77 hr	3000
	GraphCL	8.306 hr	2000
	SGRL	5.859 hr	2000
	SupGCL	21.40 hr	1500
Lung cancer	GAE	1.875 hr	1800
	GRACE	9.960 hr	3000
	GraphCL	3.303 hr	1300
	SGRL	7.485 hr	3000
	SupGCL	19.67 hr	1500
Colorectal cancer	GAE	45.23 min	2500
	GRACE	2.839 hr	3000
	GraphCL	1.476 hr	2000
	SGRL	53.14 min	1100
	SupGCL	9.551 hr	2500

We employed 10-fold cross-validation across patients to generate training/test datasets. Fine-tuning was performed using AdamW with a learning rate of 1×10^{-3} . For evaluation, we reported the mean and standard deviation of the scores across all folds.

Hazard Prediction : For the hazard prediction task, we adopted the classic Cox proportional hazards model. In the Cox model, the hazard function for a patient at time t is defined as

$$h(t | x) = h_0(t) \exp(\beta^T x)$$

Here, $h_0(t)$ is the baseline hazard, x is the input variable, and β is the regression coefficient to be learned. The prognosis estimation is performed by connecting this input variable x to the graph NN and its head.

This study performed training using partial likelihood maximization based on patient prognosis information and evaluated performance using the C-index.

Subtype Classification: For the subtype classification task, we created a classification model using a 5-class softmax function and trained it using multi-class cross-entropy. Furthermore, performance was evaluated using Accuracy and Macro F1-score. The F1-score results are shown in Appendix F.

E.3.2 Node-Level Task

For fine-tuning node-level tasks (BP/CC Classification, Cancer Rel. Classification), tasks were solved on a per-gene basis. For the latent state of each node embedded by the Graph Neural Network, task-specific models were learned through a 2-layer MLP.

In BP/CC Classification, performance was evaluated using gene-wise 10-fold cross-validation. For Cancer Rel. Classification, it is necessary to mitigate class imbalance in positive and negative label data. To achieve this, we prepared a dataset by undersampling the negative label data, split it into training and test data at an 8:2 ratio, and performed fine-tuning and accuracy evaluation. This undersampling and data splitting process was repeated 10 times with different seeds to evaluate the performance on this task.

For optimization, AdamW was used with a batch size of 8 and a learning rate of 1×10^{-3} . For evaluation, we reported the mean and standard deviation of the scores for each fold.

BP/CC. Classification : In Biological Process (BP) classification, three categories for each gene—"metabolism," "signal transduction," and "cellular organization"—are predicted as a multi-hot vector. In Cellular Component (CC) classification, four categories—"nucleus," "mitochondria," "endoplasmic reticulum," and "plasma membrane"—are predicted as a multi-hot vector. The model was structured using a sigmoid function for each category, and training was performed using binary

cross-entropy for each respective category. Performance was evaluated using Subset Accuracy, Macro F1-score, and Jaccard Index as evaluation metrics. The Macro F1-score and Jaccard Index results are shown in Appendix F.

Cancer Rel. Classification In cancer-related gene classification, 106 genes defined as positive by OncoKB were labeled as "positive," and all other genes were labeled as "negative" for binary classification. A model was created to estimate negative and positive cases using a sigmoid function, and training was performed using binary cross-entropy. Performance was evaluated using Accuracy and F1-score as evaluation metrics. The F1-score results are shown in Appendix F.

F Additional Results

As additional experimental results, we performed the following three analyses:

1. Performance evaluation of the proposed and existing methods using various evaluation metrics.
2. Visualization of the latent states of pre-trained models.
3. Performance comparison with varying embedding dimensions.

F.1 Additional Evaluation Metrics

In the main paper, we presented results using only Accuracy (or subset accuracy). Below, we report the results using other metrics for the same tasks.

Tables 10 and 11 show the Macro F1-score and Jaccard index results for node-level tasks. Please note that for the cancer-related classification task, we evaluate only the F1-score because it involves binary data. Additionally, Table 12 shows the Macro F1-score for subtype classification in breast cancer. While our proposed method, SupGCL, did not individually achieve state-of-the-art results across all tasks and metrics, it demonstrated the most balanced performance overall.

Table 10: Node-level downstream task: macro F1-score

Task	w/o-pretrain	GAE	GraphCL	GRACE	SGRL	SupGCL
BP.						
Breast	0.553±0.024	0.551±0.034	0.540±0.045	<u>0.558±0.022</u>	0.543±0.022	0.571±0.025
Lung	0.538±0.039	0.546±0.021	0.584±0.065	<u>0.555±0.026</u>	0.549±0.023	0.546±0.031
Colorectal	0.514±0.053	0.550±0.025	0.516±0.033	0.560±0.042	<u>0.560±0.040</u>	0.547±0.038
CC.						
Breast	<u>0.404±0.036</u>	0.378±0.021	0.336±0.018	0.362±0.040	0.384±0.037	0.418±0.024
Lung	0.349±0.086	0.395±0.023	0.376±0.072	<u>0.393±0.026</u>	0.385±0.026	0.387±0.028
Colorectal	0.288±0.060	0.403±0.032	0.265±0.029	0.372±0.047	<u>0.401±0.049</u>	0.397±0.030
Rel.						
Breast	0.523±0.094	0.571±0.048	<u>0.593±0.072</u>	0.591±0.038	0.578±0.067	0.610±0.070
Lung	0.507±0.117	0.559±0.045	0.538±0.236	0.535±0.139	<u>0.575±0.061</u>	0.592±0.067
Colorectal	0.474±0.242	<u>0.582±0.081</u>	0.556±0.124	0.547±0.197	0.569±0.145	0.596±0.060

F.2 Additional Latent Space Analysis

Node-level embedding of other cancers: Previously, in Result 2: Latent Space Analysis, we visualized the embedding space generated by pre-trained models on the breast cancer dataset (Figure 3). Analogous results for the lung cancer and colorectal cancer datasets are presented in Figure 4. Since subtype data were unavailable for the lung and colorectal cancer datasets, only node-level latent space visualizations are presented for these cancers. These results confirm that both GRACE and our proposed method, SupGCL, yield stable latent representations for these cancers, with no observed latent space collapse.

Table 11: Node-level downstream task: Jaccard index

Task	w/o-pretrain	GAE	GraphCL	GRACE	SGRL	SupGCL
BP.						
Breast	<u>0.490±0.017</u>	0.487±0.028	0.454±0.046	0.478±0.037	0.468±0.028	0.500±0.035
Lung	0.539±0.030	0.494±0.034	0.484±0.030	0.510±0.051	0.479±0.019	<u>0.518±0.027</u>
Colorectal	0.537±0.031	0.506±0.019	0.500±0.036	<u>0.514±0.024</u>	0.469±0.030	0.502±0.022
CC.						
Breast	<u>0.402±0.052</u>	0.378±0.021	0.303±0.028	0.359±0.028	0.377±0.029	0.422±0.028
Lung	<u>0.387±0.040</u>	0.382±0.035	0.321±0.062	0.384±0.036	0.376±0.031	0.392±0.034
Colorectal	0.377±0.055	0.379±0.036	0.308±0.067	<u>0.388±0.036</u>	0.360±0.053	0.395±0.033

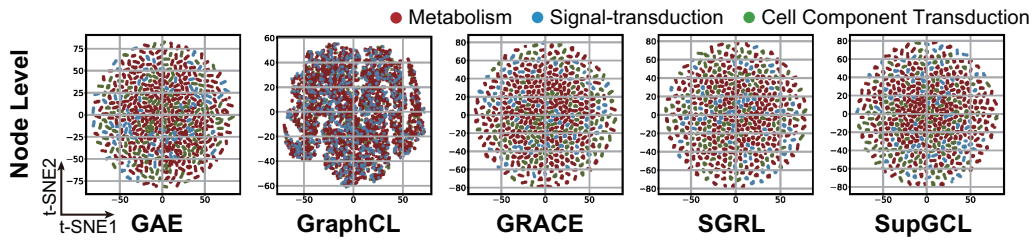
Table 12: Macro F1-score for subtype classification

Task	w/o-pretrain	GAE	GraphCL	GRACE	SGRL	SupGCL
Subtype						
Breast	0.626 ± 0.070	0.720 ± 0.057	0.552 ± 0.089	<u>0.761 ± 0.063</u>	0.715 ± 0.064	0.785 ± 0.056

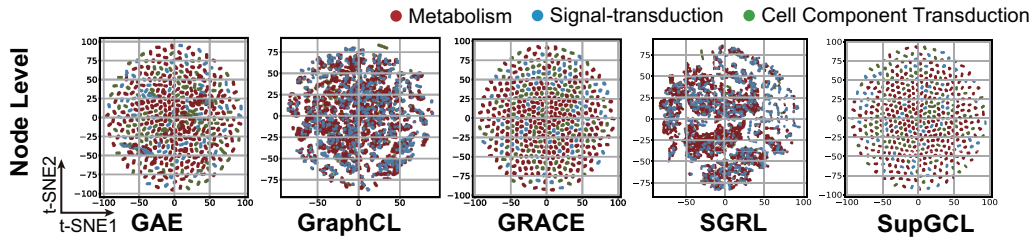
Analysis of Latent Space Collapse: To further investigate the characteristics of the node-level latent spaces presented in Result 2: Latent Space Analysis, we employed Principal Component Analysis (PCA). Figure 5 displays the PCA-projected latent spaces from pre-trained models on the breast cancer dataset, along with their corresponding explained variance ratios. For GraphCL, which previously exhibited tendencies towards latent space collapse, this analysis confirmed that its PCA explained variance ratio was overwhelmingly concentrated in the first principal component (PC1), accounting for 98.3%.

F.3 Performance Evaluation across Different Embedding Dimensions

Finally, we investigated the effect of varying embedding dimensions on performance. Figure 6 presents the performance metrics and their corresponding standard deviations across 13 tasks for embedding dimensions of {8, 16, 32, 64}. Excluding GraphCL, which exhibited instability in generating stable latent spaces, the other five methods showed only marginal performance gains when the embedding dimension was increased from 32 to 64. Furthermore, the proposed method consistently achieved high performance across all tasks and embedding dimensions, experimentally demonstrating its superiority over existing representation learning approaches for biological downstream tasks.



(a) Lung GRN



(b) Colorectal GRN

Figure 4: t-SNE visualization of pre-trained embeddings on lung and colorectal cancer GRNs.

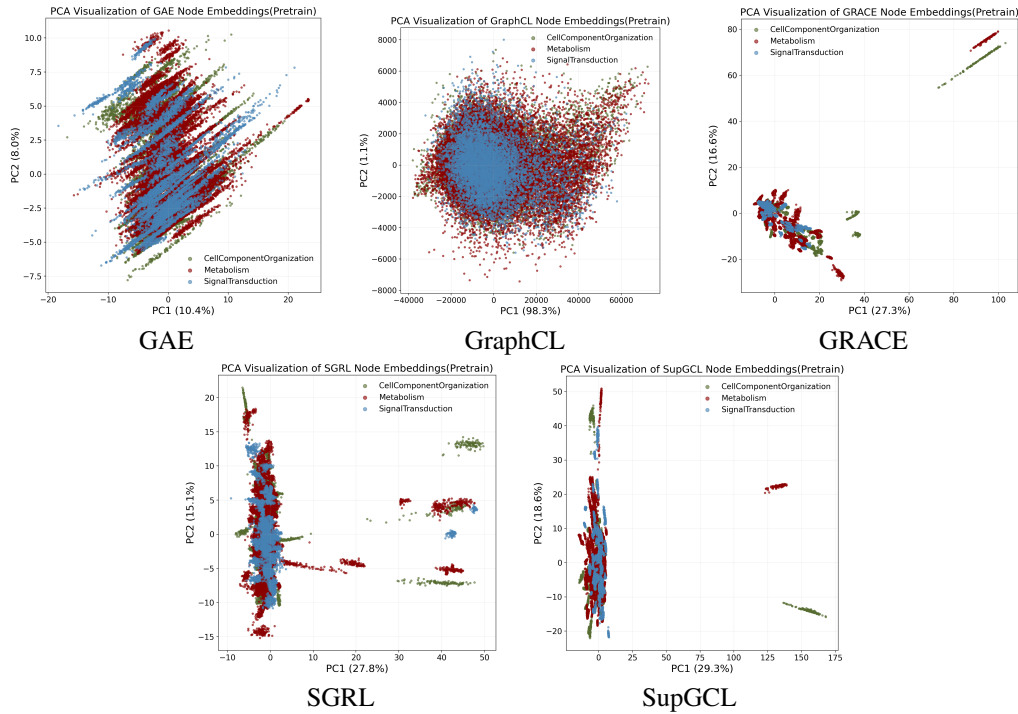


Figure 5: PCA analysis of the latent spaces of pre-trained models.

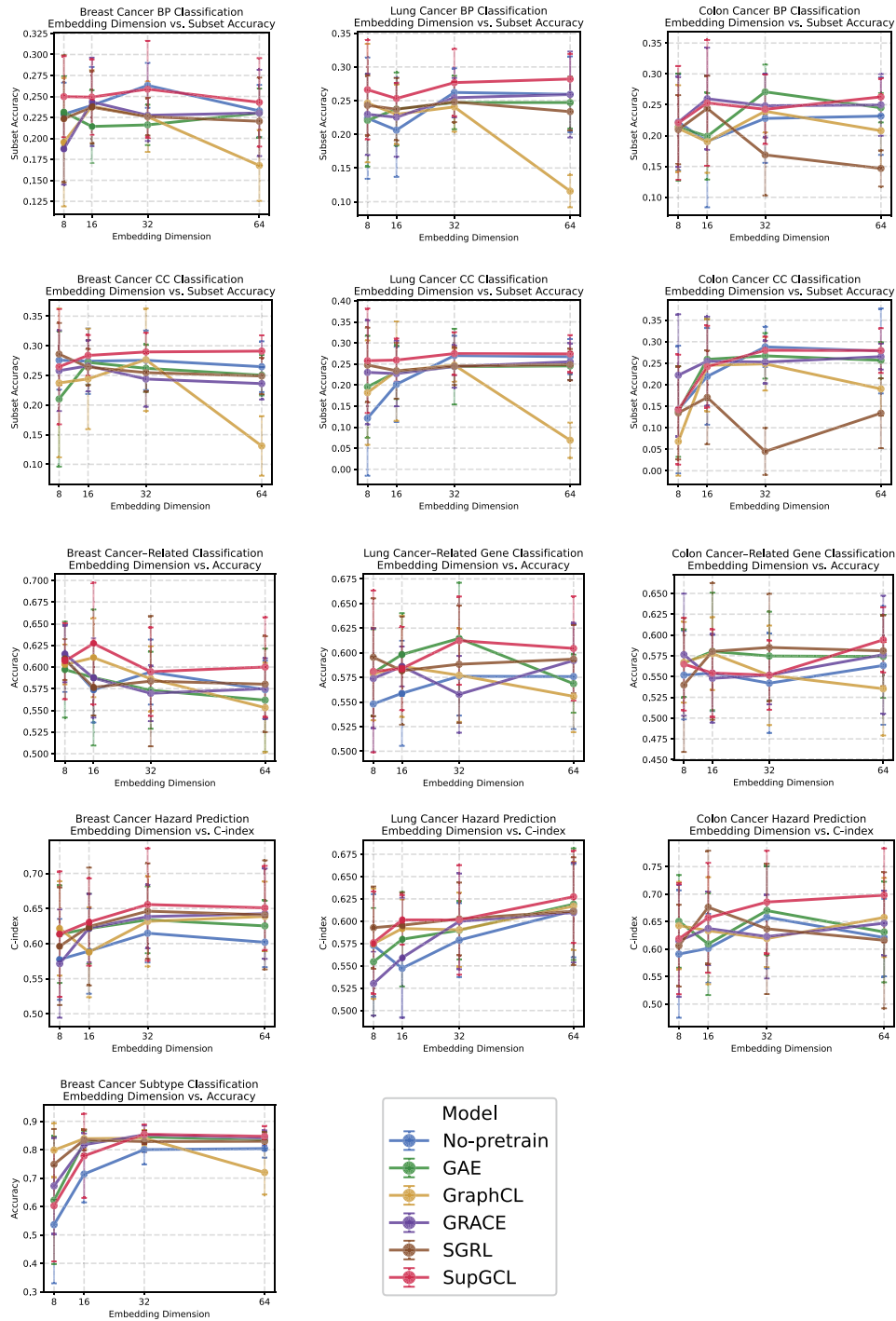


Figure 6: Embedding dimension analysis. This figure shows the performance changes across 13 tasks as the embedding dimension varies. The left column shows the results for breast cancer, the center column for lung cancer, and the right column for colorectal cancer. The first row presents the subset accuracy of BP classification, the second row shows the subset accuracy of CC classification, the third row displays the accuracy of cancer-related gene classification, the fourth row indicates the C-index for hazard prediction, and the fifth row shows the results of subtype classification.